DRAFT VERSION NOVEMBER 29, 2021
Typeset using LaTeX **twocolumn** style in AASTeX631

HD 133729: A blue large-amplitude pulsator in orbit around a main-sequence B-type star

ANDRZEJ PIGULSKI [1], KRZYSZTOF KOTYSZ [1], AND PIOTR A. KOŁACZEK-SZYMAŃSKI [1]

[1] *Astronomical Institute, Faculty of Physics and Astronomy, University of Wrocław, Kopernika 11, 51-622 Wrocław, Poland*

ABSTRACT

Blue large-amplitude pulsators (BLAPs) form a small group of hot stars pulsating with the periods of the order of 30 min. Although several scenarios of the formation of BLAPs have been proposed, we are still far from understanding the origin of these stars. Using data from Transiting Exoplanet Survey Satellite, we discovered that HD 133729 is a binary consisting of a late B-type main sequence star and a BLAP. The BLAP pulsates with a period of 32.37 min. From available photometry, we derived the times of maximum light, which revealed the binary nature of the star via $O-C$ diagram. The diagram shows variations with a period of 23.08433 d that we attribute to light-travel-time effect. The analysis of these variations allowed to derive the spectroscopic parameters of the BLAP's orbit. The presence of the hot companion in the system was confirmed by the analysis of spectral energy distribution, which was also used to place the components in Hertzsprung-Russell diagram. The obtained position of the BLAP agrees with the location of the other members of the class. With the estimated $V \approx 11$ mag and the Gaia distance of less than 0.5 kpc, the BLAP is the brightest and the nearest of all known BLAPs. It may become a clue object in the verification of the evolutionary scenarios for this class of variable. We argue that low-mass progenitors of the BLAP are excluded if the components are coeval and no mass transfer between them took place.

Keywords: stars: oscillations (including pulsations) – binaries: spectroscopic – stars: fundamental parameters – stars: individual: HD 133729

1. INTRODUCTION

Large photometric ground-based surveys provided the astronomical community with a huge number of the photometric measurements of millions of stars. Space missions were another source of a large quantity of photometric data, some with an unprecedented quality and time coverage. Although the surveys and the missions were primarily aimed at the detection of microlensing events and transiting exoplanets, the data occurred to be extremely useful in the detection and the characterisation of the different types of pulsating stars over the entire Hertzsprung-Russell (H-R) diagram. No wonder some exotic and very rare types of variable stars were found. This is the case of the discovery of the small group of short-period hot pulsators known as blue large-amplitude pulsators, hereafter BLAPs (Pietrukowicz et al. 2017).

The first BLAP was discovered serendipitously by Pietrukowicz et al. (2013) in the Optical Gravitational Lensing Experiment (OGLE) data while searching for pulsating stars in the OGLE-III Galactic disk fields in the direction tangent to the Centaurus Arm. The star, OGLE-GD-DSCT-0058, showed large-amplitude ($\Delta I = 0.24$ mag) variability and light curve resembling fundamental-mode pulsators related to δ Scuti stars, that is, high-amplitude δ Scuti stars and SX Phoenicis stars. The star was therefore tentatively classified as a δ Scuti variable. It differed from the members of these groups, however, by its exceptionally short period (28.26 min). The follow-up spectroscopic study (Pietrukowicz et al. 2015) showed that it cannot be a δ Scuti star because it is too hot; its effective temperature amounted to about 33 000 K. Searching for the other members of this group in the Galactic bulge OGLE data (Pietrukowicz et al. 2017) led to the discovery of 13 BLAPs allowing a characterisation of this new class of pulsating stars. BLAPs pulsate with periods between 22 and 40 minutes and have non-sinusoidal (a steep increase followed by a slow decrease of brightness) light curves with the peak-to-peak amplitudes of 0.2 – 0.4 mag in the V band. Amplitudes in the I band are on average about 20% lower than in the V band, which is typical for radially pulsating stars. In the H-R diagram, BLAPs are located between hot massive main-sequence stars and hot subdwarfs. Their luminosities ($\log L/\mathrm{L}_\odot = 2.2-2.6$) are, however, about an order of magnitude higher than the luminosities of hot subdwarfs, while surface gravities, $\log(g/(\mathrm{cm\,s^{-1}})) = 4.5-4.8$, are much lower than the surface gravities of hot subdwarfs. No BLAP was discovered in the Magellanic Clouds (Pietrukowicz 2018).

The existence of a separate group of pulsating stars in a poorly populated region of the H-R diagram raises a question about their origin. Pietrukowicz et al. (2017) showed that two models reproduce pulsational characteristics of BLAPs. In the first model, a BLAP has a helium-burning core with a mass of about 1 $\mathrm{M}_\odot$ and can be a descendant of a main-sequence $\sim$5 $\mathrm{M}_\odot$ star. This model was supported by the calculations of Wu & Li (2018). In the other model, a BLAP has

a degenerated helium core with a mass of $\sim$0.3 $M_\odot$ burning hydrogen in a shell. Such a configuration is typical for an evolved main-sequence star with a mass of about 1 $M_\odot$ prior to helium flash. The low-mass model was supported by Romero et al. (2018) and Córsico et al. (2018), who proposed that BLAPs are hot counterparts of pre-extremely low-mass (pre-ELM) white dwarfs (WD) with the masses of 0.27 – 0.37 $M_\odot$. This model was also favored by Byrne & Jeffery (2020). They showed that the members of the class of short-period pre-WD pulsators discovered recently by Kupfer et al. (2019) can have a similar structure as BLAPs and therefore can be deemed 'high-gravity BLAPs'. Both models proposed for BLAPs require a significant part of the initial stellar mass to be stripped off during pre-BLAP evolution. This may happen in binaries, but presently radial-velocity data do not indicate for the presence of companions to BLAPs. In this context, a model proposed by Meng et al. (2020) seemed to solve the problem. These authors showed that BLAPs can be explained as the surviving companions of type Ia supernovae, which begin their evolution as $\sim$3 $M_\odot$ stars, transfer a large part of their mass to WD companions, and end up as stars with the masses of $(0.76 \pm 0.1)\,M_\odot$ at the time of supernova explosion. Nevertheless, the origin of BLAPs is still far from being well understood.

We show in the present paper that HD 133729 is a binary with an orbital period of about 23 days consisting of a late-B spectral type main-sequence primary and a BLAP secondary. This makes the star the first known binary BLAP and a clue target for the further studies of the properties of BLAPs and evolutionary channels leading to their origin. It is also the nearest and therefore the brightest known BLAP.

2. HD 133729 AND ITS KNOWN VARIABILITY

HD 133729 is a bright ($V = 9.1$ mag) star of B6/7 V spectral type (Houk 1982). It was included in the blind search for variability among B-, A-, and F-type stars carried out by Holdsworth et al. (2014). They used data obtained within the Wide Angle Search for Planets (WASP) project (Pollacco et al. 2006). The search was focused on a discovery of short-period variability, mainly in rapidly-oscillating Ap (roAp) stars, pulsating Am stars, δ Scuti stars with high frequencies, and pre-main sequence δ Scuti stars. For HD 133729, Holdsworth et al. (2014) reported three nearly equidistant frequencies, 88.93, 88.97, and 89.02 d^{-1}, with amplitudes equal to 6, 2, and 2 mmag, respectively.

The present study shows that the dominating term found by Holdsworth et al. (2014) has frequency equal to the lowest harmonic of the real pulsation frequency. The pulsation frequency of 44.49 d^{-1} was not detected by these authors because the lower limit of their frequency search was set to 50 d^{-1}. The two other frequencies are orbital sidelobes caused by the light-travel-time effect in the system with orbital period of about 23 days (Sect. 3.3).

3. ANALYSIS OF PHOTOMETRY

3.1. *TESS photometry*

HD 133729 (TIC 75934024) was observed by the Transiting Exoplanet Survey Satellite (TESS) satellite in Sector 11 with a 2-min cadence and in Sector 38 during the TESS Extended Mission with both 2-min and 20-s cadences. The Sector 11 data were secured between 2019 April 26 and May 20, covering nearly 24 days with a 4.5-day gap in the middle of the run. The Sector 38 data were obtained between 2021 April 29 and May 26, with a short one-day gap. The data were taken from the Barbara A. Mikulski Archive for Space Telescopes (MAST) Portal[1]. We used PDCSAP fluxes in our analysis removing only some outliers and short parts at the beginning and at the end of the Sector 11 time-series.

The TESS data from both sectors were analyzed separately. Frequency spectra of the data from both sectors are fully consistent. Figure 1b shows frequency spectrum of the Sector 38 2-min cadence data. The spectrum is dominated by a frequency at $f_{\rm p} = 44.486\,d^{-1}$ and its harmonics. In addition, small-amplitude signal is present close to $2.2\,d^{-1}$. These are likely gravity modes originating in the late B-type primary. The presence of the harmonics of $f_{\rm p}$ means that the light curve is non-sinusoidal, which can be seen in Fig. 1a. A subtraction of $f_{\rm p}$ and its harmonics did not remove all signal in the vicinity of these frequencies and some residual signal was left (Fig. 1, the inset in the bottom panel). The pattern is dominated by $\pm 0.043\,d^{-1}$ sidelobes. As we show in Sect. 3.3, the sidelobes originate from phase changes caused by the orbital motion in a binary system.

The shape of the light curve of HD 133729 and its period equal to 32.37 min fit perfectly the characteristics of BLAPs. The only problem is a small peak-to-peak amplitude in TESS passband equal to about 32 parts-per-thousand (ppt). This can be explained, however, by a dilution of BLAP's light by the brighter companion. Therefore, we refer to $f_{\rm p}$ as the pulsation frequency of the BLAP.

3.2. *Archival photometry and the changes in the pulsation period*

Since BLAPs show significant period changes (Pietrukowicz et al. 2017; Wu & Li 2018; Córsico et al. 2018), we checked if this is also the case of HD 133729. This can be done because archival photometry from Hipparcos space mission and two ground-based surveys, All-Sky Automated Survey (ASAS, Pojmański 1997, 2000, 2009), and WASP (Pollacco et al. 2006), is available for this star. The details of the data and the derivation of pulsation frequencies are given in Appendix A.

Figure 5 in Appendix A shows the resulting changes in the pulsation frequency, which at first approximation can be assumed linear. The derived rate of frequency change, $df_{\rm p}/dt = (1.41 \pm 0.07) \times 10^{-7}\,d^{-2}$, translates into the rate of period change $dP_{\rm p}/dt \equiv \dot{P}_{\rm p} = (-7.11 \pm 0.33) \times 10^{-11}$ or $r \equiv \dot{P}_{\rm p}/P_{\rm p} = (-11.5 \pm 0.6) \times 10^{-7}\,({\rm yr})^{-1}$, where $P_{\rm p} = f_{\rm p}^{-1}$ is the pulsation period. This is the largest negative value of

[1] https://mast.stsci.edu/portal/Mashup/Clients/Mast/Portal.html

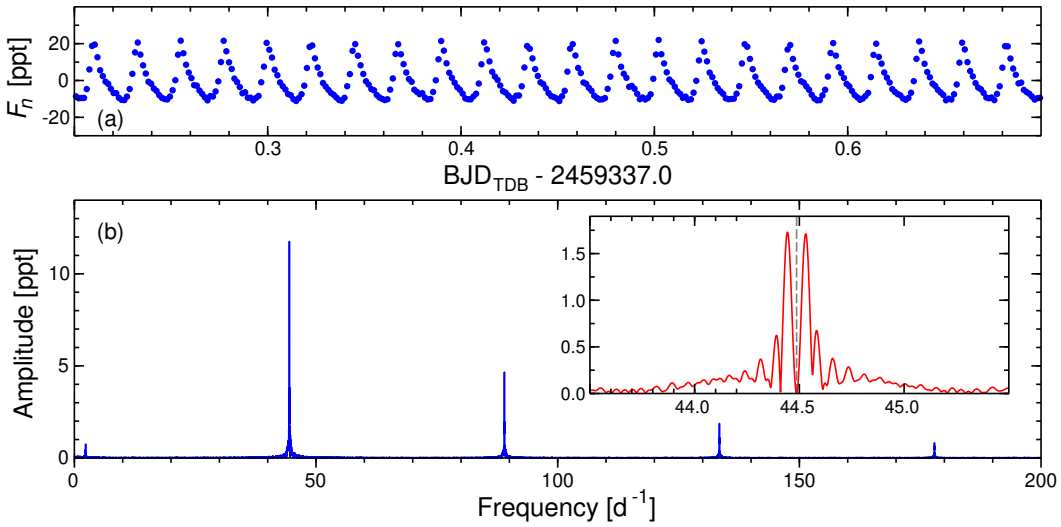

Figure 1. Light curve and frequency spectrum of the TESS data of HD 133729. (a) Half-day 2-minute cadence TESS Sector 38 light curve of HD 133729. $F_{\rm n}$ stands for the relative flux $F_i/\langle F\rangle - 1$, where F_i is the TESS flux for the ith data point and $\langle F\rangle$ is average flux from all TESS observations in Sector 38. (b) Frequency spectrum of the TESS Sector 38 data. In order to illustrate the occurrence of the $\pm 0.043\,{\rm d}^{-1}$ orbital sidelobes, the inset shows $2\,{\rm d}^{-1}$-wide frequency spectrum of the residuals in the vicinity of $f_{\rm p} = 44.487\,{\rm d}^{-1}$, after subtracting $f_{\rm p}$ and its harmonics.

the rate of the period change of all known BLAPs, if the uncertain value of $\dot{P}_{\rm p}$ for OGLE-BLAP-002 derived by Wu & Li (2018) is not taken into account.

3.3. *Light-travel-time effect*

A periodic photometric signal sent by a component of a binary can serve as a clock and be used to derive the same orbital parameters that are derived for a single-lined spectroscopic binary. The involved effect is usually called the light-travel-time effect (hereafter LTTE) and results in the occurrence of orbital sidelobes in frequency spectra at a separation equal to an orbital frequency, $f_{\rm orb}$. For HD 133729, a separation of orbital sidelobes, equal to about $0.043\,{\rm d}^{-1}$ (Fig. 1), indicates for an orbital period of $P_{\rm orb} = f_{\rm orb}^{-1} \approx 23$ days.

Figure 2d shows the superb quality of the TESS data. It can be also seen that the average light curves for the 2-min cadence Sector 11 and Sector 38 data look the same. Since the 2-min cadence TESS data are sufficient for an $O-C$ analysis, we did not use the 20-s cadence data for this purpose. However, these data were analyzed in the same way as the 2-min cadence data and, for completeness, the phase-averaged light curve for these data is shown in Fig. 2d. In general, the 20-s cadence data are consistent with the 2-min cadence data. The only difference is an unusual tiny drop of flux in the light curve of the 20-s cadence data at phase 0.05 lasting only about 40 s. The feature is not visible in the 2-min cadence light curve due to averaging. It may have the same origin as a small drop at maximum light that was found in OGLE-BLAP-009 (Pietrukowicz et al. 2017; McWhirter et al. 2020).

In order to analyze LTTE, we used the times of maximum light of the pulsation of the BLAP (Fig. 2). Since data used to derive a single time of maximum light have to cover a reasonably small part of the orbital period, the only data suitable for this kind of an analysis are the TESS and the WASP data. Appendix B explains how the times of maximum light, given in Table 3, were derived.

Having obtained the times of maximum light, $T^O_{\rm max}$, we used them to generate $O-C$ diagram shown in Fig. 3a. The values of $O-C$ were calculated with respect to the following ephemeris:

$$C(E) = T^C_{\rm max}(E) = {\rm BJD_{TDB}}\,2\,453\,860.487 + 0.022478855 \times E, \quad (1)$$

where E is the number of pulsation periods elapsed from the initial epoch. The values of $O-C = T^O_{\rm max} - T^C_{\rm max}$, where $T^O_{\rm max}$ and $T^C_{\rm max}$ stand for the observed and the calculated times of maximum light, respectively. They are given in Table 3. The $O-C$ diagram shows periodic variation with the period of about 23 d superimposed on changes on a much longer time scale. As expected, the changes on a long-time scale reflect to some extent the decrease of pulsation period derived in Appendix A, but it is also obvious that a constant rate of period change, represented by the dashed-line parabola, does not fit the observations well. The real changes in the pulsation period are more complicated. Unfortunately, they cannot be traced by the available photometry because of the gaps in the data. Since we are interested in the periodic variation in the $O-C$ diagram, we subtracted the long term changes seen in Fig. 3a, separately for the WASP and the TESS data, by fitting 'locally' and subtracting parabolae with quadratic terms corresponding to $\dot{P}_{\rm p} = -7.11 \times 10^{-11}$ (Sect. 3.2). These parabolae are shown with the dotted lines in Fig. 3a.

Residual $O-C$ values, $(O-C)_{\rm res}$, were used to derive parameters of the orbit of the BLAP by fitting equation

$$(O-C)_{\rm res}(t) = \tau(a_2 \sin i, P_{\rm orb}, T_0, e, \omega, t) + {\rm const} \quad (2)$$

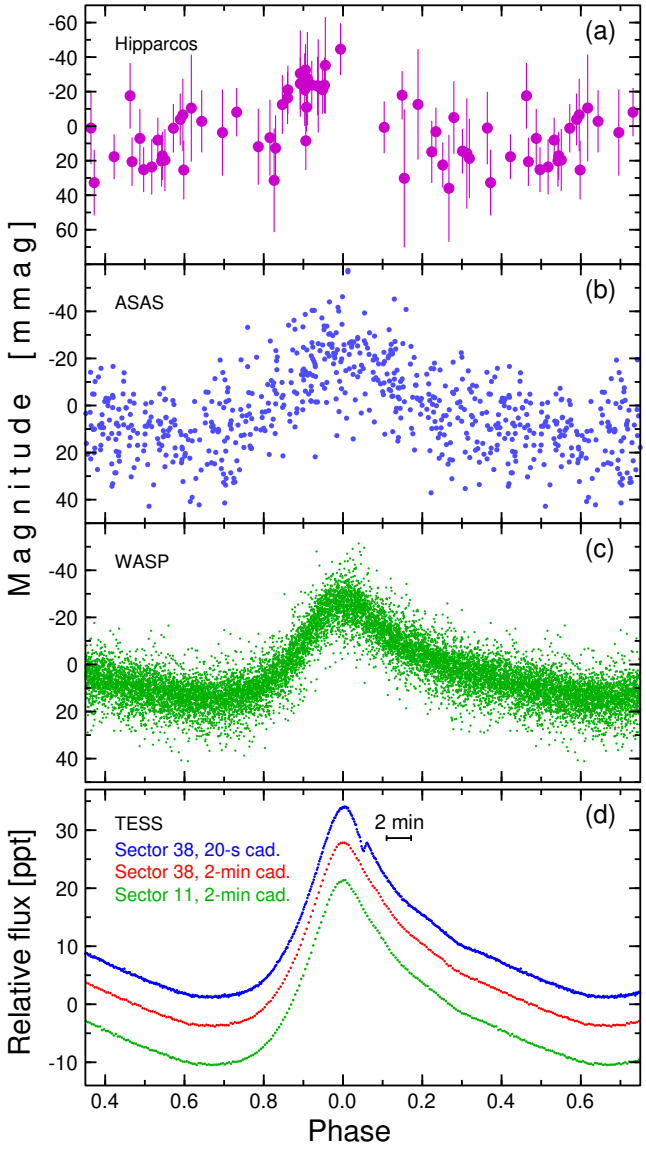

Figure 2. Light curves of HD 133729 phased with the pulsation period. (a)–(c) Hipparcos (a), ASAS (b), and WASP (c) light curves. (d) Phase-averaged TESS light curves in Sector 11 (green dots), Sector 38, 2-min cadence (red dots), and Sector 38, 20-s cadence (blue dots). For clarity, 5 ppt offsets were applied between the light curves. The 2-min cadence data are averaged in 0.005, the 20-s cadence data, in 0.002 phase intervals. Phase 0.0 corresponds to the time of maximum light.

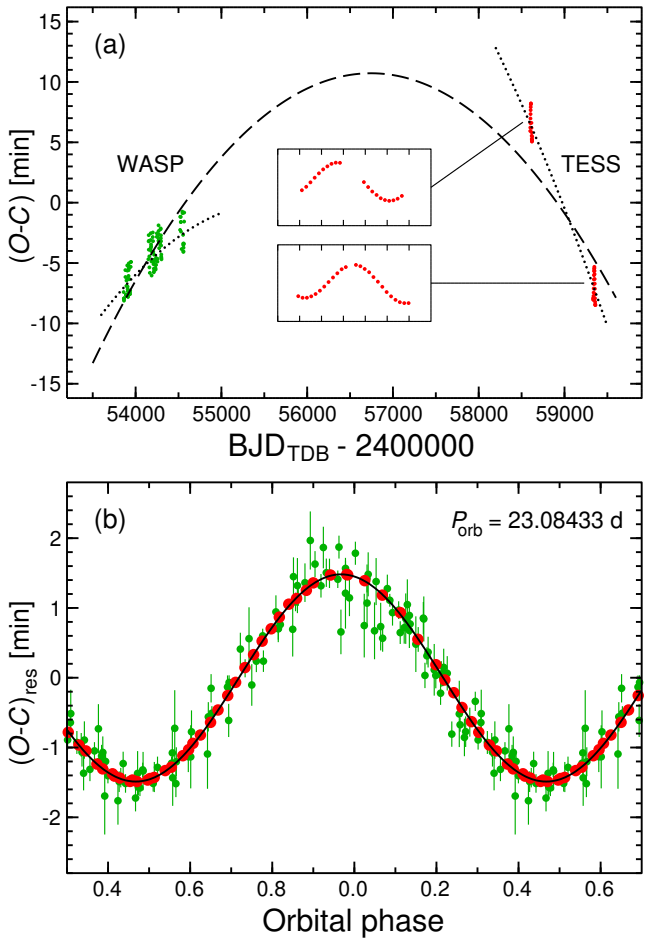

Figure 3. $O-C$ diagrams for the pulsation period of HD 133729. (a) $O-C$ diagram for the WASP (green dots) and the TESS (red dots) times of maximum light obtained using Eq. (1) as a reference. Dashed line shows a fit with the assumed rate of period change $\dot{P}_{\rm p} = -7.11 \times 10^{-11}$ derived in Appendix A. Dotted lines show fits of parabolae with the same $\dot{P}_{\rm p}$ separately to the WASP and the TESS data. Ordinate ranges one pulsation period. The two insets show zoomed TESS data, the abscissa ticks are separated by 5 d. (b) Residuals from the fits shown in the upper panel phased with the orbital period of 23.08433 d. Red and green dots correspond to the TESS and the WASP data, respectively. Solid black line is a fit of Eq. (2) to the residual $O-C$ data. Parameters of the fit are given in Table 1. Phase 0.0 corresponds to T_0.

to the residual data. The values of $(O-C)_{\rm res}$ are also given in Table 3. In Eq. (2), the light-travel time τ is defined by the eq. (3) of Irwin (1952). Derived parameters are listed in Table 1. The residual $O-C$ values phased with the derived orbital period are shown in Fig. 3b. The orbit is marginally eccentric. Although the WASP data resulted in the much less precise times of maximum light than the TESS data, they are important for constraining $P_{\rm orb}$, because they increase the span of data to about 240 orbital cycles. The high precision of K_2[2] and mass function $f(M_1)$ is the result of the precise determination of the amplitude of LTTE, which in turn is a consequence of the high precision of the times of maximum light derived from the TESS data. The standard deviation of residuals from the fit shown in Fig. 3b amounts to 16.0 s for the WASP data and only 0.7 s for the TESS data.

[2] We consequently use subscript '1' and name 'primary' for the late B-type component, and subscript '2' and name 'secondary' for the BLAP.

Table 1. Parameters of the orbit of BLAP derived from fitting the $O-C$ diagram.

Parameter	Value
Orbital period, $P_{\rm orb}$	23.08433 ± 0.00023 d
Time of periastron passage, T_0	BJD $2\,453\,900.4 \pm 1.2$
Eccentricity, e	0.0055 ± 0.0017
Argument of periastron, ω	$102 \pm 19^\circ$
Projected major semiaxis of the secondary's absolute orbit, $a_2 \sin i$	38.389 ± 0.032 R$_\odot$
Half-range of the secondary's radial-velocity variation, K_2	84.13 ± 0.07 km s^{-1}
Mass function, $f(M_1)$	1.424 ± 0.004 M$_\odot$

4. SED FITTING AND THE PARAMETERS OF THE COMPONENTS

In order to verify if the multi-band photometry of HD 133729 is consistent with the system consisting of a late B-type star and a BLAP, we performed spectral energy distribution (SED) analysis using VOSA[3] on-line tool (Bayo et al. 2008). We used Tycho $B_{\rm T}$ and $V_{\rm T}$ (Høg et al. 2000) and Gaia G, $G_{\rm bp}$, and $G_{\rm rp}$ (Gaia Collaboration et al. 2018) photometry in the optical domain. In the infrared (IR) domain, we selected photometry in Two Micron All-Sky Survey (2MASS) $JHK_{\rm s}$ (Cutri et al. 2003) and Wide-field Infrared Survey Explorer (WISE) $W1$, $W2$, and $W3$ (Cutri & et al. 2012) passbands. Assuming that the contribution of the BLAP in the optical and IR domains is small compared to the contribution of the B-type primary, we obtained a best-fit model with the effective temperature $T_{\rm eff,1} = 11\,500$ K and the surface gravity $\log(g_1/({\rm cm\,s^{-2}})) = 4.0$ dex. We assumed total absorption in Johnson V band $A_V = 0.386$ mag and total-to-selective absorption ratio $R_V = 3.1$. The value of A_V was taken from the Gaia-2MASS three-dimensional map of absorption presented by Lallement et al. (2019) using their on-line tool[4]. During a standard least-squares fitting procedure, we used Castelli-Kurucz ODFNEW/NOVER synthetic spectra (Castelli et al. 1997) and assumed solar metallicity. The fit is shown in Fig. 4a, the residuals, in Fig. 4b. The plots show also another source of photometric data, ultraviolet (UV) fluxes collected by Thor-Delta 1A (TD-1) satellite in four passbands, 156.5, 196.5, 236.5 and 274.0 nm (Thompson et al. 1978, 1995). They were not used in the fit because the contribution of the BLAP in UV is significant. The star is barely detected in the three longest-wavelength TD-1 passbands because the errors are larger than the measured fluxes, but in the 156.5-nm band the flux amounts to $(5.25\pm0.49)\times10^{-14}$ W m^{-2} (nm)$^{-1}$. The comparison of the ratios of TD-1 fluxes to those of the fitted SED model shows clearly (Fig. 4b) that the observed flux in the 156.5-nm band is roughly three times higher than expected from a late B-type star. This can be explained only by the presence of a hot secondary, the BLAP. We therefore took a spectrum with parameters representing known BLAPs, $T_{\rm eff,2} = 29\,000$ K and $\log(g_2/({\rm cm\,s^{-2}})) = 4.5$ dex, and scaled it to obtain the best fit of the combined spectrum to the TD-1 observations. The result is shown in Fig. 4a with a black line. It can be seen that adding a hot companion to the fit, we obtained a satisfactory agreement in the whole range of the available passbands.

The SEDs of both components allowed us to estimate a relative contribution of the components in different passbands. In particular, the BLAP contribution to the total flux of the system amounts to about 19% in Johnson V and 16% in the TESS band. The latter value allows to estimate the intrinsic amplitude of the BLAP. The observed peak-to-peak amplitude of the BLAP in the TESS band amounts to 31.6 ppt, which translates into the intrinsic amplitude of 0.21 mag, in full agreement with the I-filter amplitudes of BLAPs derived by Pietrukowicz et al. (2017).

In order to locate the components of the system in the H-R diagram, we used the results of the SED fitting. The measured Gaia Early Data Release 3 parallax of HD 133729 amounts to 2.136 ± 0.029 mas, which translates into the distance of 463 ± 7 pc (Bailer-Jones et al. 2021). We calculated V magnitude of the system translating Tycho $B_{\rm T}$ and $V_{\rm T}$ magnitudes by means of eq. (1) of Oja & Evans (1998). It is equal to 9.174 mag. In consequence, we obtained $V_1 \approx 9.37$ mag and $V_2 \approx 11.0$ mag adopting the relative contributions of the components estimated from the SED fitting. This results in the absolute magnitude of the primary equal to $M_{V,1} = +0.66$ mag. Adopting bolometric correction $({\rm BC})_{V,1} = -0.596$ mag, calculated from the equation provided by Pedersen et al. (2020) for Johnson V band, assuming $T_{\rm eff,1} = 11\,500$ K, and $M_{\rm bol,\odot} = 4.74$ mag, we obtained the bolometric magnitude of the primary $M_{\rm bol,1} = +0.06$ mag and its luminosity $\log(L_1/{\rm L}_\odot) = 1.87 \pm 0.12$. In these calculations, an uncertainty of ±1000 K for $T_{\rm eff,1}$ was adopted. As can be seen in Fig. 4a, this value encompasses all photometric data and small differences in the visual and IR domains between the spectrum of the primary and the combined spectrum. Uncertainty of $\log(L_1/{\rm L}_\odot)$ depends on the uncertainties of four parameters: distance, V_1, A_V, and $({\rm BC})_{V,1}$. Adopting $\sigma(A_V) = 0.1$ mag, $\sigma(V_1) = 0.15$ mag, and $\sigma(({\rm BC})_{V,1}) = 0.25$ mag, we obtained the uncertainty of $\log(L_1/{\rm L}_\odot)$ equal to 0.12 dex. A comparison of the location of the primary with the evolutionary models (Fig. 4c) places the star in the main sequence phase of evolution, as expected from its luminosity class. The inferred mass of the primary amounts to (2.85 ± 0.25) M$_\odot$.

The SED fitting allowed us to estimate the relative luminosities of the components by integrating the SEDs of both components. A relative luminosity, $L_2/L_1 \approx 1.9$, combined with the luminosity of the primary derived above gives $\log(L_2/{\rm L}_\odot) = 2.15 \pm 0.15$. Along with the sec-

[3] http://svo2.cab.inta-csic.es/theory/vosa/

[4] https://astro.acri-st.fr/gaia_dev/

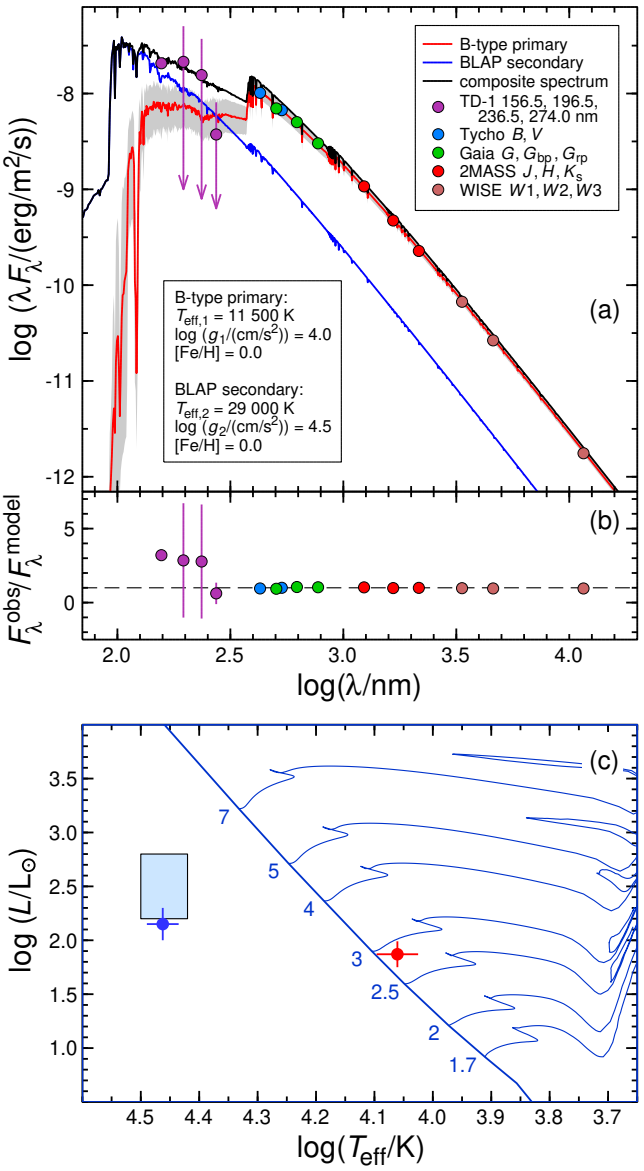

Figure 4. Results of SED fitting and H-R diagram for the components of HD 133729. (a) SED fitting. The color-coded points with error bars stand for the observed fluxes de-reddened by the VOSA tool. The spectrum fitted to the optical and the IR data is shown with solid red curve. The shaded area marks the effect of ± 1000 K uncertainty in $T_{\rm eff,1}$. The adopted spectrum of the BLAP scaled to account for the UV data is marked with blue line. The composite spectrum of the binary is shown with black line. (b) Residuals from fitting SED to the visual and IR photometry of HD 133729 in the terms of flux ratio. (c) Positions of the components of HD 133729 in the H-R diagram. The B-type primary is marked with red dot, the BLAP, with blue dot. Light blue rectangle shows the position of BLAPs as defined by Pietrukowicz et al. (2017). Evolutionary tracks, labeled with mass in $M_\odot$, and the zero-age main sequence line were taken from the non-rotating models of Ekström et al. (2012).

ondary's effective temperature adopted for the SED fitting ($T_{\rm eff,2} = 29\,000$ K), this allows to plot the position of the secondary in the H-R diagram. As can be seen in Fig. 4c, it fits within the errors the 'instability strip' of BLAPs defined by Pietrukowicz et al. (2017). The location and the size of the strip is still rather uncertain. It may extend towards lower luminosities, especially if BLAPs and high-gravity BLAPs form a homogeneous group. The location of the secondary in the H-R diagram is another argument in the favor of the recognition of the star as a BLAP.

5. DISCUSSION AND CONCLUSIONS

BLAPs are very rare objects. Only 14 were discovered during the extensive survey of the OGLE data by Pietrukowicz et al. (2017) and Pietrukowicz (2018). Adding four high-gravity BLAPs found by Kupfer et al. (2019), which may belong to the same class, and one candidate with the period of 18.9 min found recently by Lin et al. (2021), the secondary of HD 133729 is only the 20th member of the class. This star is unusual for several reasons. First, because it is the only known BLAP that resides in a binary. The binary is wide enough to make use of the light-travel-time effect for the determination of precise spectroscopic elements of its orbit (Sect. 3.3). Next, it is the nearest and the brightest star of this type. With the estimated $V \approx 11.0$ mag (Sect. 4), it is almost 5 mag brighter than the next brightest BLAP, OGLE-BLAP-009 ($V \approx 15.7$ mag). Finally, the unusual short-living feature in the descending branch of the light curve (Fig. 2) is exceptional among radially pulsating stars.

In an obvious way, the discovery of a BLAP in a bright binary system prompts for a detailed follow-up spectroscopic study, which we are going to carry out. First of all, this should provide the mass ratio of the components. Given the relatively tight constraint on M_1 (Sect. 4), with the relative error of the order of 10%, this should allow to constrain M_2 with a comparable precision. For this purpose, we need to measure precisely K_1, the half-range of the primary's radial-velocity variation. In this context, the domination of the primary in the optical part of the spectrum of the system might be a favorable circumstance. We already know K_2 with a 0.1% precision from the $O-C$ analysis (Table 1). Such a precision of K_2 would be hardly achievable from the analysis of optical spectra, as the secondary contributes only 15 – 20% to the optical spectrum and its lines would be affected by the presence of short-period large-amplitude pulsations. A precise value of mass ratio, allowing to constrain also the mass of the secondary, should allow to conclude on the evolutionary status of this BLAP and choose between scenarios leading to a shell-hydrogen-burning star with a mass of $0.3-0.4\,M_\odot$ and those that predict a core-helium-burning star with a higher mass of $0.5-1.0\,M_\odot$.

If a coevality of both components is assumed and no mass transfer onto the primary took place, the progenitor of the BLAP in the HD 133729 system must have started its evolution with an initial mass larger than $\sim 3\,M_\odot$. This would exclude evolutionary scenarios that lead to low-mass BLAPs, because they start with a $\sim 1\,M_\odot$ progenitors. A detailed dis-

cussion of the possible evolutionary scenarios of this BLAP is, however, beyond the scope of this paper, and is postponed to the spectroscopic study.

The publication of this paper was partially financed by the University of Wrocław program 'Initiative of Excellence – Research University'. AP, KK, and PKS were supported by the National Science Centre (NCN) grants no. 2016/21/B/ST9/01126, 2019/33/N/ST9/01818, and 2019/35/N/ST9/03805, respectively. This work used the SIMBAD and Vizier services operated by Centre des Données astronomiques de Strasbourg (France), and bibliographic references from the Astrophysics Data System maintained by SAO/NASA. This paper makes use of data from the DR1 of the WASP data (Butters et al. 2010) as provided by the WASP consortium, and the computing and storage facilities at the CERIT Scientific Cloud, reg. no. CZ.1.05/3.2.00/08.0144, which is operated by Masaryk University, Czech Republic. This publication makes use of VOSA, developed under the Spanish Virtual Observatory project supported from the Spanish MICINN through grant AyA2008-02156. This work has made use of data from the European Space Agency (ESA) mission *Gaia* (https://www.cosmos.esa.int/gaia), processed by the *Gaia* Data Processing and Analysis Consortium (DPAC, https://www.cosmos.esa.int/web/gaia/dpac/consortium). Funding for the DPAC has been provided by national institutions, in particular the institutions participating in the *Gaia* Multilateral Agreement. Some of the data presented in this paper were obtained from the MAST at the Space Telescope Science Institute. STScI is operated by the Association of Universities for Research in Astronomy, Inc., under NASA contract NAS5-26555. Support for MAST for non-HST data is provided by the NASA Office of Space Science via grant NAG5-7584 and by other grants and contracts. This paper includes data collected by the TESS mission, which are publicly available from the MAST.

REFERENCES

Bailer-Jones, C. A. L., Rybizki, J., Fouesneau, M., Demleitner, M., & Andrae, R. 2021, AJ, 161, 147, doi: 10.3847/1538-3881/abd806

Bayo, A., Rodrigo, C., Barrado Y Navascués, D., et al. 2008, A&A, 492, 277, doi: 10.1051/0004-6361:200810395

Butters, O. W., West, R. G., Anderson, D. R., et al. 2010, A&A, 520, L10, doi: 10.1051/0004-6361/201015655

Byrne, C. M., & Jeffery, C. S. 2020, MNRAS, 492, 232, doi: 10.1093/mnras/stz3486

Castelli, F., Gratton, R. G., & Kurucz, R. L. 1997, A&A, 318, 841

Córsico, A. H., Romero, A. D., Althaus, L. G., Pelisoli, I., & Kepler, S. O. 2018, arXiv e-prints, arXiv:1809.07451. https://arxiv.org/abs/1809.07451

Cutri, R. M., & et al. 2012, VizieR Online Data Catalog, II/311

Cutri, R. M., Skrutskie, M. F., van Dyk, S., et al. 2003, VizieR Online Data Catalog, II/246

Eastman, J., Siverd, R., & Gaudi, B. S. 2010, PASP, 122, 935, doi: 10.1086/655938

Ekström, S., Georgy, C., Eggenberger, P., et al. 2012, A&A, 537, A146, doi: 10.1051/0004-6361/201117751

ESA. 1997, in ESA Special Publication, Vol. 1200

Gaia Collaboration, Brown, A. G. A., Vallenari, A., et al. 2018, A&A, 616, A1, doi: 10.1051/0004-6361/201833051

Høg, E., Fabricius, C., Makarov, V. V., et al. 2000, A&A, 355, L27

Holdsworth, D. L., Smalley, B., Gillon, M., et al. 2014, MNRAS, 439, 2078, doi: 10.1093/mnras/stu094

Houk, N. 1982, Michigan Catalogue of Two-dimensional Spectral Types for the HD stars. Volume 3. Declinations −40° to −26° (University of Michigan)

Irwin, J. B. 1952, ApJ, 116, 211, doi: 10.1086/145604

Kupfer, T., Bauer, E. B., Burdge, K. B., et al. 2019, ApJL, 878, L35, doi: 10.3847/2041-8213/ab263c

Lallement, R., Babusiaux, C., Vergely, J. L., et al. 2019, A&A, 625, A135, doi: 10.1051/0004-6361/201834695

Lin, J., Wang, X., Mo, J., et al. 2021, MNRAS, doi: 10.1093/mnras/stab2812

McWhirter, P. R., Lam, M. C., & Steele, I. A. 2020, MNRAS, 496, 1105, doi: 10.1093/mnras/staa1560

Meng, X.-C., Han, Z.-W., Podsiadlowski, P., & Li, J. 2020, ApJ, 903, 100, doi: 10.3847/1538-4357/abbb8e

Oja, T., & Evans, D. W. 1998, A&A, 333, 673

Pedersen, M. G., Escorza, A., Pápics, P. I., & Aerts, C. 2020, MNRAS, 495, 2738, doi: 10.1093/mnras/staa1292

Pietrukowicz, P., Dziembowski, W. A., Mróz, P., et al. 2013, AcA, 63, 379. https://arxiv.org/abs/1311.5894

Pietrukowicz, P. 2018, in The RR Lyrae 2017 Conference. Revival of the Classical Pulsators: from Galactic Structure to Stellar Interior Diagnostics, ed. R. Smolec, K. Kinemuchi, & R. I. Anderson, Vol. 6, 258–262. https://arxiv.org/abs/1802.04405

Pietrukowicz, P., Latour, M., Angeloni, R., et al. 2015, AcA, 65, 63. https://arxiv.org/abs/1503.03499

Pietrukowicz, P., Dziembowski, W. A., Latour, M., et al. 2017, Nature Astronomy, 1, 0166, doi: 10.1038/s41550-017-0166

Pojmański, G. 1997, AcA, 47, 467. https://arxiv.org/abs/astro-ph/9712146

—. 2000, AcA, 50, 177. https://arxiv.org/abs/astro-ph/0005236

Pojmański, G. 2009, in Astronomical Society of the Pacific Conference Series, Vol. 403, The Variable Universe: A Celebration of Bohdan Paczynski, ed. K. Z. Stanek, 52

Pollacco, D. L., Skillen, I., Collier Cameron, A., et al. 2006, PASP, 118, 1407, doi: 10.1086/508556

Romero, A. D., Córsico, A. H., Althaus, L. G., Pelisoli, I., & Kepler, S. O. 2018, MNRAS, 477, L30, doi: 10.1093/mnrasl/sly051

Thompson, G. I., Nandy, K., Jamar, C., et al. 1978, Catalogue of stellar ultraviolet fluxes: a compilation of absolute stellar fluxes measured by the Sky Survey Telescope (S2/68) aboard the ESRO satellite TD-1 (The Science Research Council, U.K.)

—. 1995, VizieR Online Data Catalog, II/59B

Wu, T., & Li, Y. 2018, MNRAS, 478, 3871, doi: 10.1093/mnras/sty1347

APPENDIX

A. DERIVATION OF PULSATION FREQUENCIES

The archival photometry of HD 133729 from the Hipparcos mission, the ASAS survey, and the WASP survey, was first cleaned from outliers and the data of lower quality. Since we were interested in the the light curve of the BLAP, we also removed some obvious trends in photometry by filtering out low frequencies. In order to account for phase changes due to the orbital motion, the archival time-series photometry $m(t)$ was fitted with the following variability model:

$$m(t) = m_0 + \sum_{n=1}^{N} \{A_n \sin(2\pi n f_{\rm p} t + \phi_n) + A_{n-} \sin[2\pi(n f_{\rm p} - f_{\rm orb})t + \phi_{n-}] + A_{n+} \sin[2\pi(n f_{\rm p} + f_{\rm orb})t + \phi_{n+}]\}. \quad \text{(A1)}$$

Parameters derived in this model are amplitudes A_n, A_{n-}, and A_{n+}, phases ϕ_n, ϕ_{n-}, and ϕ_{n+}, pulsation frequency $f_{\rm p}$, orbital frequency $f_{\rm orb}$, and mean magnitude m_0. The value of N depended on the number of harmonics of $f_{\rm p}$ detected in a given data set. We adopted $N = 2$ for the Hipparcos and ASAS data, and $N = 4$ for the WASP data. For the TESS data, we had to proceed in a different way, because the data are short and each sector covers only about one orbital period. Therefore, we first derived the parameters of the orbit (Sect. 3.3), then corrected the times of observations according to the formula given by Irwin (1952) accounting for the light-travel-time delay, and only then fitted a simplified model consisting of only $f_{\rm p}$ and its harmonics up to $N = 12$, that is, without the two terms containing orbital sidelobes in Eq. (A1). The values of $f_{\rm p}$ derived from the fits are listed in Table 2 and plotted in Fig. 5. Light curves from all surveys phased with the pulsation period, are presented in Fig. 2.

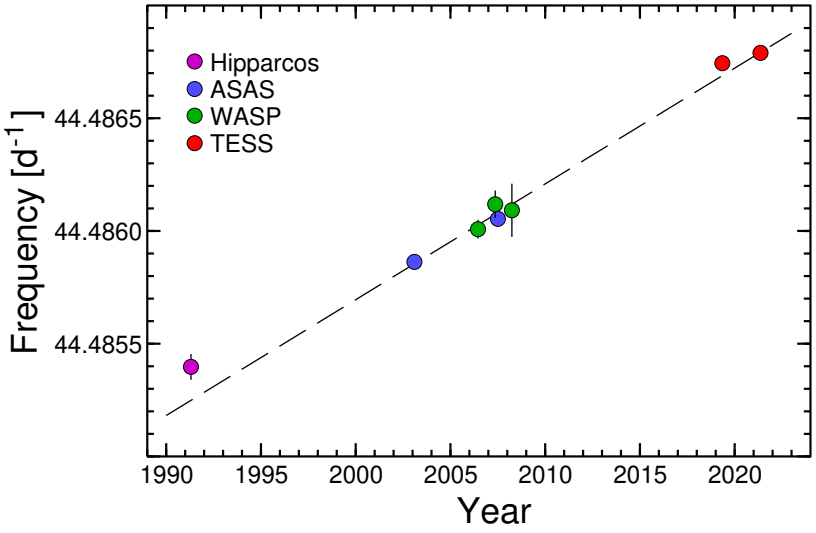

Figure 5. Pulsation frequencies of the BLAP in the HD 133729 system derived from the Hippaarcos, ASAS, WASP, and TESS data. Dashed line corresponds to the derived constant rate of frequency change, $\mathrm{d}f_{\rm p}/\mathrm{d}t = (1.41 \pm 0.07) \times 10^{-7}\,\mathrm{d}^{-2}$.

The Hipparcos photometry of HD 133729 (HIP 73969) is very scarce (Fig. 2), so that the detection of $f_{\rm p}$ is marginal, but it is very important from the point of view of monitoring the changes in the pulsation period, because the data extend the time span of photometric data of HD 133729 to ∼30 years. The star was deemed constant in the Hipparcos catalog (ESA 1997).

The ASAS V-filter data of the star (ASAS 150658-3138.7) were downloaded from the ASAS web page[5]. They cover almost nine years between December 2000 and September 2009. Therefore, we split the ASAS data into two equal parts, which resulted in two points in Fig. 5.

The WASP data of HD 133729 were downloaded from the public database[6]. Over 11 000 original data points were available for the star, designated as 1SWASP J150658.93-313838.9. The data span three seasons, between 2006 and 2008. For the purpose of the determination of $f_{\rm p}$, each season was analyzed separately, which resulted in three points in Fig. 5.

[5] http://www.astrouw.edu.pl/asas/?page=aasc

[6] https://wasp.cerit-sc.cz/form

Table 2. Pulsation frequencies $f_{\rm p}$ derived from fitting Eq. (A1) to the available photometric data.

Source of data	Mean time [year]	$N_{\rm obs}{}^a$	N^a	$f_{\rm p}$ [d^{-1}]
Hipparcos	1991.307	53	2	44.48540(6)
ASAS, part 1	2003.100	256	2	44.485864(17)
ASAS, part 2	2007.505	257	2	44.486053(17)
WASP, part 1	2006.456	2998	4	44.48601(4)
WASP, part 2	2007.362	5131	4	44.48612(6)
WASP, part 3	2008.243	1378	4	44.48609(12)
TESS, sector 11	2019.350	13808	12	44.486742(11)
TESS, sector 38	2021.363	17926	12	44.486792(9)

[a] $N_{\rm obs}$ stands for the number of observations, N is the number of harmonics in Eq. (A1).

B. DERIVATION OF THE TIMES OF MAXIMUM LIGHT

The TESS data were split into ∼1-day long subsets. This resulted in 45 subsets, 20 for Sector 11 and 25 for Sector 38 observations. Then, a smoothed light curve was obtained by phasing the Sector 38 2-min cadence TESS light curve (Fig. 2). Next, the smoothed light curve was fitted to each subset separately by means of the least squares. In effect, a single time of maximum light was obtained for each subset. It was the closest to the mid-time of observations. A similar procedure was applied to the WASP data, but in this case we chose subsets corresponding to individual nights. Nights with less than 20 data points were excluded. In this way, 117 times of the maximum light for the WASP data were obtained. The times of observations in the WASP data are given in Heliocentric Julian Days (HJD), while for the TESS data, in Barycentric Julian Days in the standard of Barycentric Dynamical Time, TDB (BJD$_{\rm TDB}$). In order to make them consistent, we converted the WASP times of maximum light to BJD$_{\rm TDB}$ using the on-line tool[7] provided by J. Eastman (Eastman et al. 2010). All times of maximum light, $T_{\rm max}$, are given in Table 3 as BJD$_{\rm TDB}$ − 2 450 000.0. The meaning of E, $(O-C)$, and $(O-C)_{\rm res}$ is explained in Sect. 3.3.

Table 3. Times of maximum light obtained using the WASP data and the TESS 2-min cadence data.

$T_{\rm max}$	E	$(O-C)$ [d]	$(O-C)_{\rm res}$ [d]	$T_{\rm max}$	E	$(O-C)$ [d]	$(O-C)_{\rm res}$ [d]
3860.48186(15)	0	−0.00514	−0.00054	4270.29687(31)	18231	−0.00214	0.00052
3862.43715(11)	87	−0.00551	−0.00091	4271.33077(13)	18277	−0.00226	0.00039
3863.44864(7)	132	−0.00557	−0.00097	4272.31990(11)	18321	−0.00220	0.00045
3864.43764(9)	176	−0.00564	−0.00105	4273.33139(12)	18366	−0.00227	0.00038
3865.40437(7)	219	−0.00550	−0.00092	4274.32010(12)	18410	−0.00262	0.00002
3880.39939(9)	886	−0.00388	0.00062	4286.41404(16)	18948	−0.00231	0.00028
3881.38806(8)	930	−0.00428	0.00022	4287.31307(10)	18988	−0.00242	0.00016
3886.39982(9)	1153	−0.00530	−0.00083	4291.24777(14)	19163	−0.00153	0.00104
3887.38887(11)	1197	−0.00532	−0.00085	4292.32680(7)	19211	−0.00148	0.00109

Table 3 *continued*

[7] https://astroutils.astronomy.osu.edu/time/hjd2bjd.html

Table 3 *(continued)*

$T_{\max}$	E	$(O-C)$ [d]	$(O-C)_{\rm res}$ [d]	$T_{\max}$	E	$(O-C)$ [d]	$(O-C)_{\rm res}$ [d]
3890.37860(14)	1330	−0.00528	−0.00084	4294.30437(23)	19299	−0.00205	0.00051
3892.37971(6)	1419	−0.00479	−0.00035	4295.31609(8)	19344	−0.00188	0.00067
3893.34661(7)	1462	−0.00448	−0.00005	4296.28234(27)	19387	−0.00222	0.00033
3902.38397(6)	1864	−0.00361	0.00077	4297.31612(25)	19433	−0.00247	0.00008
3903.48514(17)	1913	−0.00391	0.00047	4298.30456(12)	19477	−0.00310	−0.00056
3904.36138(12)	1952	−0.00435	0.00002	4299.31623(14)	19522	−0.00298	−0.00044
3905.35044(9)	1996	−0.00436	0.00001	4300.30510(11)	19566	−0.00318	−0.00064
3906.33903(6)	2040	−0.00483	−0.00047	4301.29409(8)	19610	−0.00326	−0.00073
3907.35044(9)	2085	−0.00498	−0.00062	4518.55391(10)	29275	−0.00157	0.00016
3909.32846(15)	2173	−0.00509	−0.00074	4520.46537(27)	29360	−0.00081	0.00092
3910.33976(9)	2218	−0.00534	−0.00099	4525.52310(13)	29585	−0.00082	0.00089
3911.32874(8)	2262	−0.00543	−0.00109	4526.55684(25)	29631	−0.00112	0.00059
3913.23980(25)	2347	−0.00507	−0.00075	4527.54591(16)	29675	−0.00111	0.00059
3916.34255(11)	2485	−0.00440	−0.00009	4528.55691(12)	29720	−0.00166	0.00004
3917.33181(9)	2529	−0.00421	0.00009	4536.53590(27)	30075	−0.00267	−0.00100
3918.32121(7)	2573	−0.00388	0.00042	4544.54052(12)	30431	−0.00052	0.00113
3919.31040(6)	2617	−0.00377	0.00053	4547.53012(21)	30564	−0.00061	0.00103
3920.32222(8)	2662	−0.00349	0.00080	4553.55320(9)	30832	−0.00185	−0.00023
3926.27885(15)	2927	−0.00376	0.00050	4554.51929(14)	30875	−0.00236	−0.00074
3927.38040(22)	2976	−0.00367	0.00059	4555.53076(7)	30920	−0.00244	−0.00083
3928.32378(11)	3018	−0.00440	−0.00015	4556.54191(23)	30965	−0.00283	−0.00122
3934.36983(22)	3287	−0.00517	−0.00095	4557.53101(13)	31009	−0.00280	−0.00120
3935.24641(8)	3326	−0.00526	−0.00105	4558.58773(14)	31056	−0.00259	−0.00099
3936.28064(6)	3372	−0.00506	−0.00085	4560.49864(15)	31141	−0.00238	−0.00079
3942.28386(10)	3639	−0.00369	0.00049	4561.57766(34)	31189	−0.00235	−0.00076
3943.25073(9)	3682	−0.00342	0.00075	4565.55768(13)	31366	−0.00109	0.00049
3947.27445(21)	3861	−0.00341	0.00074	4566.41239(19)	31404	−0.00057	0.00101
4148.55027(20)	12815	−0.00326	−0.00007	8600.517360(9)	210866	0.004122	−0.000653
4151.54099(19)	12948	−0.00222	0.00095	8601.506628(9)	210910	0.004320	−0.000444
4152.57537(20)	12994	−0.00187	0.00130	8602.473475(8)	210953	0.004576	−0.000177
4153.56361(22)	13038	−0.00270	0.00046	8603.440333(9)	210996	0.004843	0.000101
4155.54226(23)	13126	−0.00219	0.00096	8604.407175(9)	211039	0.005095	0.000364
4159.54260(17)	13304	−0.00309	0.00004	8605.373993(8)	211082	0.005322	0.000603
4160.50856(18)	13347	−0.00372	−0.00059	8606.340758(8)	211125	0.005496	0.000788
4165.52103(19)	13570	−0.00404	−0.00093	8607.285015(8)	211167	0.005641	0.000944
4171.47927(31)	13835	−0.00269	0.00039	8608.251673(7)	211210	0.005708	0.001022
4175.52600(11)	14015	−0.00215	0.00092	8609.218254(7)	211253	0.005699	0.001024

Table 3 *continued*

Table 3 *(continued)*

$T_{\max}$	E	$(O-C)$ [d]	$(O-C)_{\rm res}$ [d]	$T_{\max}$	E	$(O-C)$ [d]	$(O-C)_{\rm res}$ [d]
4176.53794(11)	14060	−0.00176	0.00130	8614.679507(9)	211496	0.004590	−0.000022
4178.53774(28)	14149	−0.00258	0.00047	8615.645813(8)	211539	0.004305	−0.000296
4179.54947(12)	14194	−0.00240	0.00065	8616.589667(7)	211581	0.004047	−0.000543
4180.53843(10)	14238	−0.00251	0.00053	8617.578539(8)	211625	0.003850	−0.000728
4181.54970(15)	14283	−0.00278	0.00026	8618.522462(7)	211667	0.003660	−0.000907
4184.53879(23)	14416	−0.00338	−0.00036	8619.488950(7)	211710	0.003558	−0.000998
4186.44868(38)	14501	−0.00419	−0.00118	8620.455495(8)	211753	0.003512	−0.001033
4199.55607(8)	15084	−0.00198	0.00098	8621.422116(7)	211796	0.003542	−0.000992
4200.54540(11)	15128	−0.00171	0.00124	8622.388797(7)	211839	0.003633	−0.000890
4203.46716(25)	15258	−0.00221	0.00073	8623.355550(7)	211882	0.003795	−0.000716
4205.51212(18)	15349	−0.00283	0.00010	9334.689629(7)	243527	−0.005492	−0.000956
4206.38833(33)	15388	−0.00329	−0.00036	9335.678610(7)	243571	−0.005582	−0.001032
4207.60211(10)	15442	−0.00337	−0.00045	9336.667680(7)	243615	−0.005581	−0.001018
4208.38870(18)	15477	−0.00354	−0.00062	9337.656829(7)	243659	−0.005501	−0.000924
4211.51280(8)	15616	−0.00400	−0.00110	9338.646033(7)	243703	−0.005367	−0.000776
4212.50207(10)	15660	−0.00379	−0.00089	9339.635295(7)	243747	−0.005175	−0.000570
4213.53595(13)	15706	−0.00395	−0.00105	9340.624600(7)	243791	−0.004939	−0.000321
4214.41314(21)	15745	−0.00343	−0.00054	9341.613931(7)	243835	−0.004678	−0.000046
4215.51504(14)	15794	−0.00299	−0.00011	9342.625741(8)	243880	−0.004416	0.000230
4216.50379(16)	15838	−0.00331	−0.00042	9343.615054(8)	243924	−0.004173	0.000487
4231.42930(17)	16502	−0.00377	−0.00095	9344.604356(8)	243968	−0.003941	0.000732
4232.44102(10)	16547	−0.00359	−0.00078	9345.593549(8)	244012	−0.003817	0.000870
4233.42984(10)	16591	−0.00385	−0.00103	9347.864040(7)	244113	−0.003691	0.001028
4236.55494(37)	16730	−0.00330	−0.00050	9348.875513(7)	244158	−0.003767	0.000966
4237.45382(31)	16770	−0.00358	−0.00079	9349.864424(7)	244202	−0.003925	0.000822
4238.44329(14)	16814	−0.00318	−0.00039	9350.875784(8)	244247	−0.004113	0.000648
4246.37954(18)	17167	−0.00196	0.00080	9351.864576(8)	244291	−0.004391	0.000383
4247.36881(13)	17211	−0.00177	0.00099	9352.875857(8)	244336	−0.004658	0.000130
4254.38058(11)	17523	−0.00339	−0.00067	9353.887113(8)	244381	−0.004951	−0.000149
4255.34734(24)	17566	−0.00323	−0.00051	9354.875881(7)	244425	−0.005253	−0.000437
4265.32916(16)	18010	−0.00202	0.00065	9355.887182(7)	244470	−0.005500	−0.000670
4266.27310(27)	18052	−0.00219	0.00048	9356.898528(7)	244515	−0.005703	−0.000859
4267.26306(28)	18096	−0.00130	0.00137	9357.887463(8)	244559	−0.005837	−0.000979
4268.34172(14)	18144	−0.00163	0.00104	9358.898958(8)	244604	−0.005890	−0.001018
4269.24068(35)	18184	−0.00182	0.00084	9359.888029(7)	244648	−0.005889	−0.001003

Facilities: TESS, ASAS, WASP, Gaia, Hipparcos, TD-1, 2MASS, WISE, Tycho

Software: VOSA (Bayo et al. 2008), hjd2bjd (https://astroutils.astronomy.osu.edu/time/hjd2bjd.html)